ChemComm

Multi-color luminescent crystals derived from dynamic diastereomers of a perylene-substituted binaphthol derivative

Journal:	*ChemComm*
Manuscript ID	CC-COM-02-2025-000758.R2
Article Type:	Communication

ChemComm

COMMUNICATION

Multi-color luminescent crystals derived from dynamic diastereomers of a perylene-substituted binaphthol derivative

Riko Yano[a] and Suguru Ito*[ab]

Received 00th January 20xx,
Accepted 00th January 20xx

DOI: 10.1039/x0xx00000x

Herein, we demonstrate a novel strategy for obtaining multi-color luminescent crystals. A perylene-substituted (*S*)-binaphthol derivative was designed, exhibiting dynamic conversion of diastereomers in solution. Crystallization of the dynamic mixture yielded three crystals with different emission colors, each having a different composition of diastereomers and solvent molecules.

Controlling the luminescent properties of organic crystals has recently attracted increasing interest, as these are expected to find a wide range of optoelectronic applications.[1] The primary approach to producing multi-color luminescent crystals involves the synthesis of derivatives bearing sterically or electronically different substituents, as well as the extension or reduction of π-conjugation systems.[2] However, multi-step synthetic and purification processes are laborious and costly. An alternative strategy for achieving multi-color luminescence is to prepare polymorphs or solvent-including crystals from a single luminescent compound, as the emission color of organic molecular crystals varies depending on molecular conformation and intermolecular interactions.[3] In these crystals, distinct luminescent properties arise from variations in π-stacking modes between intermolecular luminophores[4] or differences in dihedral angles between intramolecular (hetero)aromatic rings.[5] Moreover, the emission properties of luminescent organic crystals can be modulated by external stimuli that induce phase transitions into another polymorph or an amorphous state. Such stimuli-responsive properties are promising for applications in multi-color devices, sensors, and security materials. Therefore, rational molecular design strategies for intentionally obtaining multi-color luminescent crystals from a single compound are of critical importance for advancing optoelectronic organic materials.

Recently, intriguing enantioselective and diastereoselective crystallizations have been reported for equilibrium mixtures of stereoisomers resulting from dynamic chirality.[6] For example, the equilibrium between the *P*- and *M*-enantiomers of a compound can be suppressed upon crystallization with an enantiopure *S*-form guest, producing crystals consisting of the *M*-enantiomer and the *S*-guest (Fig. 1a).[6d] Similarly, dynamic diastereomers between the *S*,*P*- and *S*,*M*-forms can yield crystals composed of both diastereomers (Fig. 1b) or a single diastereomer (Fig. 1c).[6a] However, in the previous report, these two types of diastereomeric crystals (Fig. 1b and 1c) were selectively obtained from different compounds. We hypothesized that multiple crystals with different emission colors could be obtained when the dynamic diastereomers of a single luminescent compound produce both types of diastereomeric crystals as well as solvent-including crystals.

We have designed (*S*)-**1**, in which a perylene ring is substituted at the 3-position of (*S*)-2,2′-dimethoxy-1,1′-binaphthol (BINOL) dimethyl ether. Due to the rotation of the chiral axis between the naphthalene and perylene rings, (*S*)-**1** is expected to interconvert between two diastereomers (*S*,*S*)-**1** and (*S*,*R*)-**1** in solution. Upon crystallization, the rotation of the chiral axis is expected to be restricted. When (*S*)-**1** was crystallized from various solvents, three types of luminescent crystals were obtained, each consisting of different combinations of the isomers and solvent molecules. These crystals exhibited different emission colors depending on the stacking arrangement of the perylene rings and underwent emission color changes in response to mechanical and thermal stimuli (Fig. 1d).

Perylene-substituted BINOL derivative (*S*)-**1** was synthesized in 72% yield via Suzuki–Miyaura coupling using (*S*)-(2,2′-dimethoxy-[1,1′-binaphthalen]-3-yl)boronic acid[7] and 3-bromoperylene[8] (Scheme S1). In the ^{1}H NMR spectrum of (*S*)-**1**

[a] *Department of Chemistry and Life Science, Graduate School of Engineering Science, Yokohama National University, 79-5 Tokiwadai, Hodogaya-ku, Yokohama 240-8501, Japan. E-mail: suguru-ito@ynu.ac.jp*
[b] *PRESTO, Japan Science and Technology Agency (JST), 4-1-8 Honcho, Kawaguchi, Saitama 332-0012, Japan.*

† Electronic supplementary information (ESI) available: Synthesis, NMR spectra, theoretical calculations, crystal structures, and luminescence properties. See DOI: 10.1039/x0xx00000x

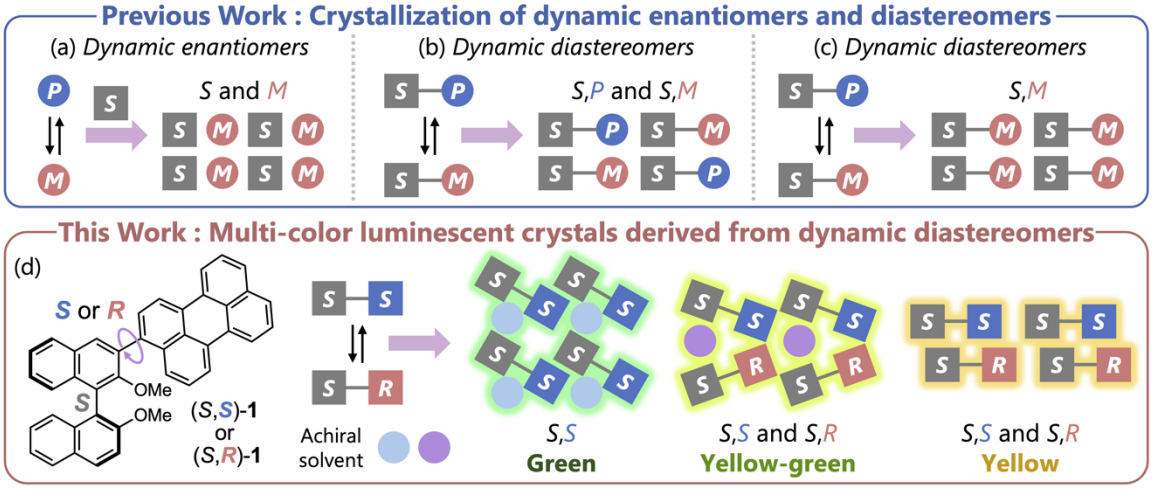

Fig. 1 (a) Crystallization of dynamic enantiomers with *S*-guest produces crystals consisted of *M*-enantiomer and *S*-guest. Crystallization of dynamic diastereomers produces crystals consisted of (b) two diastereomers or (c) a single diastereomer. (d) Crystallization of dynamic diastereomers (*S*,*S*)-**1** and (*S*,*R*)-**1** produces three luminescent crystals.

in DMSO-d_6 at room temperature, the non-equivalent methyl groups Me(a) and Me(b) each exhibited two signals, suggesting the presence of two diastereomers (*S*,*S*)-**1** and (*S*,*R*)-**1** (Fig. 2). Compared with Me(a), the signals of Me(b) were observed upfield, probably due to the shielding effect of the perylene ring. The difference in the chemical shift values between (*S*,*S*)-**1** and (*S*,*R*)-**1** was 0.066 ppm for Me(a) and 0.095 ppm for Me(b) (Fig. S1, ESI†). The diastereomeric ratio (*S*,*S*)-**1**/(*S*,*R*)-**1** was 1:1.2.

The diastereomers (*S*,*S*)-**1** and (*S*,*R*)-**1** were assigned based on the comparison between experimental and calculated NMR signals (Fig. S2 and Table S1, ESI†). Calculations for ^{1}H NMR signals in $CDCl_3$ suggested that the signal of Me(a) in (*S*,*R*)-**1** appears at downfield relative to (*S*,*S*)-**1**, whereas the signal of Me(b) in (*S*,*R*)-**1** appears upfield. The calculated ^{13}C NMR signals further supported the assignment of (*S*,*S*)-**1** and (*S*,*R*)-**1**.

With increasing temperature, the ^{1}H NMR signals of both diastereomers approached and coalesced at 140 °C (Fig. 2 and Fig. S1, ESI†). The free energy of activation for bond rotation, calculated from the variable-temperature ^{1}H NMR spectra, was 88 kJ/mol, indicating that the chiral axis is rotatable at room temperature, although too slow to be averaged on the NMR time scale.

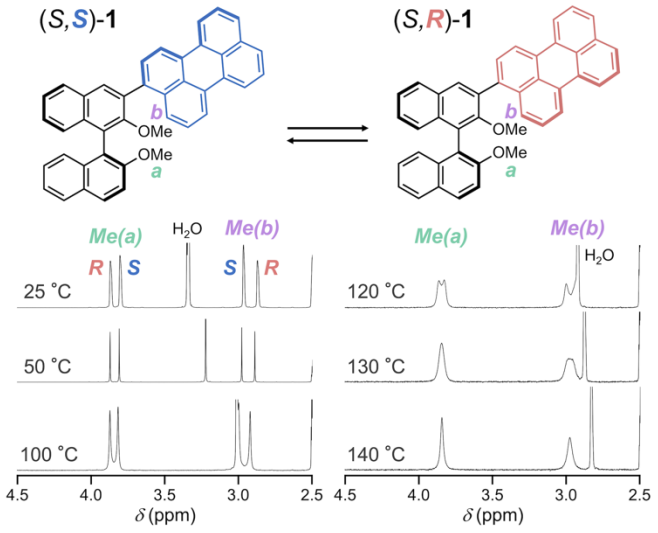

Fig. 2 Variable-temperature ^{1}H NMR spectra of Me(a) and Me(b) in the dynamic diastereomers (*S*,*S*)-**1** and (*S*,*R*)-**1** in DMSO-d_6.

Three types of crystals with different emission colors were obtained by vapor diffusion of methanol into a dynamic mixture of (*S*,*S*)-**1** and (*S*,*R*)-**1** in various organic solvents (Table S2). Green-emissive crystal **G** (λ_{em} = 515 nm, Φ_F = 0.21), yellow-green-emissive crystal **YG** (λ_{em} = 523 nm, Φ_F = 0.18), and yellow-emissive crystal **Y** (λ_{em} = 577 nm, Φ_F = 0.07) were obtained from 1,4-dioxane, toluene, and ethyl acetate solutions, respectively (Fig. 3 and Fig. S3–6, ESI†). Crystal **Y** could also be obtained by recrystallization from a hot toluene–methanol solution (Fig. S7, ESI†). The absorption spectra of **G**, **YG**, and **Y** were almost identical, whereas mirror-image CD spectra were observed in **G** (Fig. S8 and S9, ESI†). In various solvents, (*S*)-**1** exhibited blue emission regardless of solvent polarity (Fig. S10, ESI†). In the aggregated state, the absorption spectrum was red-shifted, resulting in yellow-green emission from the amorphous state (Fig. S11–S13, ESI†). These results suggest that the emission colors of the crystals vary depending on molecular arrangements in the crystalline state.

The structures of the three types of crystals were elucidated by single-crystal X-ray diffraction analysis (Fig. 3, Fig. S3–S5, and Table S2, ESI†). Both **G** and **YG** included solvent molecules. Specifically, **G** (space group: $P2_12_12_1$) was composed solely of diastereomer (*S*,*S*)-**1** and included equimolar amounts of 1,4-dioxane molecules, and **YG** (space group: $P2_1$) contained (*S*,*S*)-**1**, (*S*,*R*)-**1**, and toluene molecules in a molar ratio of 1:1:1. In contrast, **Y** (space group: *P*1), which was composed exclusively of (*S*,*S*)-**1** and (*S*,*R*)-**1**, contained no solvent molecules.

In **G** and **YG**, the perylene rings of adjacent molecules were spatially isolated, whereas in **Y**, two perylene rings were stacked. In **G**, the dihedral angle between adjacent perylene rings was 26.75°, and the distance between one perylene ring and the

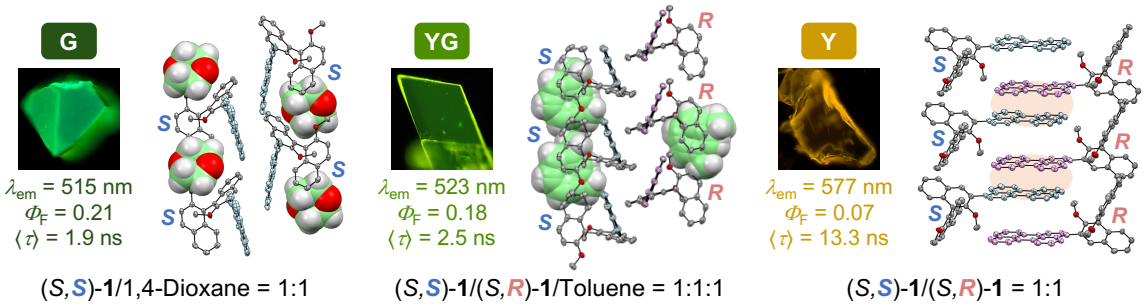

Fig. 3 Luminescence properties and crystal structures of **G**, **YG**, and **Y**. The molecular structures of (*S*,*S*)-**1** and (*S*,*R*)-**1** are shown with atomic displacement parameters set at 50% probability (Color code: light blue and pink = perylene, dark gray = C, red = O). All hydrogen atoms are omitted for clarity, except those in 1,4-dioxane and toluene molecules, which are depicted in the CPK model (Color code: light green = C, light gray = H, red = O).

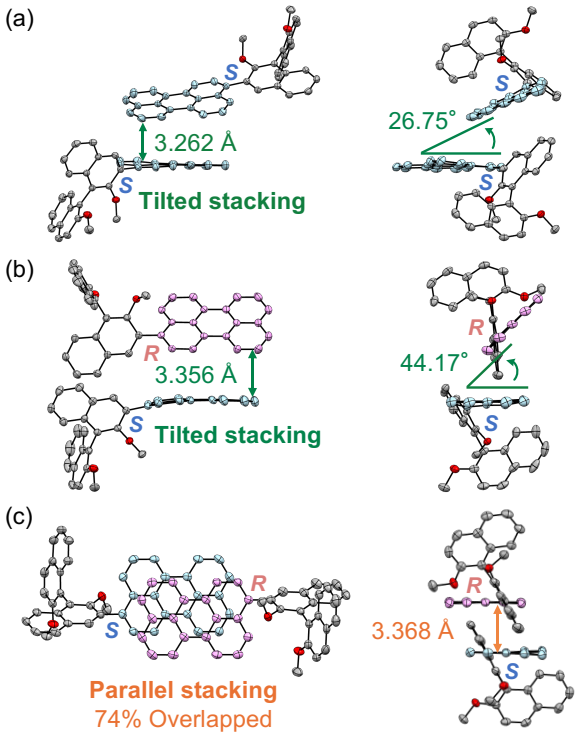

Fig. 4 Front and side views of the two adjacent molecules in the crystal structures of (a) **G**, (b) **YG**, and (c) **Y**.

closest carbon atom of the other perylene ring was 3.262 Å (Fig. 4a). In **YG**, the distance between the perylene rings of (*S*,*S*)-**1** and (*S*,*R*)-**1** was 3.356 Å, with a dihedral angle of 44.17° (Fig. 4b). In contrast, in **Y**, the perylene rings of (*S*,*S*)-**1** and (*S*,*R*)-**1** were stacked, with an overlapping area of 74% (Fig. 4c). Therefore, the green to yellow-green emission of **G** and **YG** arises from the monomer emission of perylene ring, whereas the yellow emission of **Y** originates from the excimer emission of perylene ring. The fluorescence lifetimes of **G** ($\langle\tau\rangle$ = 1.9 ns) and **YG** ($\langle\tau\rangle$ = 2.5 ns) were comparable to that of the monomer emission of a reported perylene derivative ($\langle\tau\rangle$ = 3.9 ns).[9] In contrast, **Y** exhibited a longer lifetime ($\langle\tau\rangle$ = 13.3 ns) (Fig. S14 and Table S3, ESI†), which corresponds to the excimer emission of perylene from the stacked dimer, as confirmed by X-ray analysis.

The three crystals changed their emission colors in response to mechanical stimuli. Upon grinding with a spatula, all crystals transitioned to yellow-green-emissive states (λ_{em} = 545–550 nm, Φ_F = 0.16–0.26) (Fig. 5a). Powder X-ray diffraction (PXRD) of **G** showed a decrease in peak intensity after grinding, indicating a phase transition to an amorphous state (Fig. 5b). The yellow-green-emissive amorphous state exhibited a longer lifetime ($\langle\tau\rangle$ = 13.3 ns) than the monomer emission, suggesting excimer emission (Fig. S14 and Table S3, ESI†). The increase in fluorescence quantum yield is attributed to a reduced nonradiative decay rate compared with **G**. Similarly, the ground **YG** was an amorphous state that exhibits excimer emission ($\langle\tau\rangle$ = 12.7 ns) with suppressed nonradiative decay processes. In contrast, upon grinding **Y**, the fluorescence rate constant increased, leading to excimer emission ($\langle\tau\rangle$ = 11.0 ns) with a higher fluorescence quantum yield.

The ground state also changed emission color in response to heat or solvent exposure. When the ground state was heated to 210 °C, yellow emission was observed, with the PXRD pattern

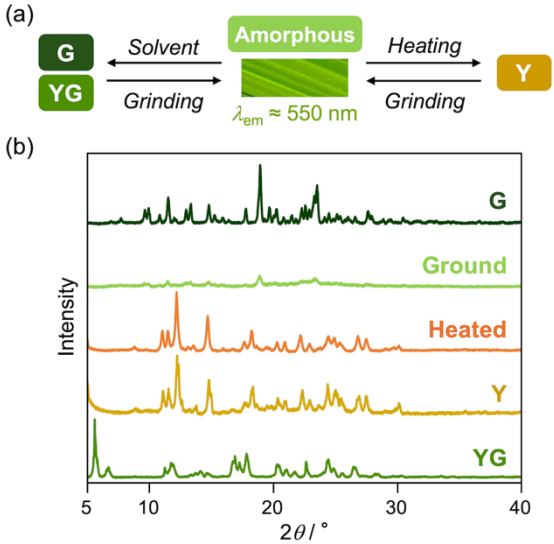

Fig. 5 (a) Interconversion between crystalline and amorphous states in response to grinding, solvent exposure, and heating. (b) PXRD patterns of **G**, after grinding **G**, after heating ground **G**, **Y**, and **YG**.

matching that of **Y** (Fig. 5b and Fig. S15, ESI†). Furthermore, when 1,4-dioxane was dropped onto the ground state and subsequently air-dried, green-emissive crystals were formed (λ_{em} = 504 nm) (Fig. S16a, ESI†). Similarly, treatment with toluene restored the amorphous state to **YG** (Fig. S16b, ESI†).

When crystalline **G** was heated to 180 °C, the emission color changed from green to yellow-green and then to yellow (Fig. S17a, ESI†). This change was attributed to the amorphization caused by the release of the solvent, followed by the transition from the amorphous state to **Y** at 180 °C (Fig. S18a, ESI†). A similar phenomenon was observed when crystalline **YG** was heated to 210 °C. PXRD patterns also supported the stepwise transitions of **YG** upon heating (Fig. S17b and S18b, ESI†).

In conclusion, we designed and synthesized the perylene-substituted BINOL derivative (*S*)-**1** and obtained three types of luminescent crystals **G**, **YG**, and **Y** from various solvents. In solution, the two diastereomers (*S*,*S*)-**1** and (*S*,*R*)-**1** were in equilibrium owing to the rotation of the chiral axis at the 3-position of the naphthalene ring, while the dynamic chirality was suppressed upon crystallization. The ability of (*S*)-**1** to adopt stable diastereomers despite high conformational flexibility would be a major factor contributing to its crystallization into distinct phases. Crystal structure analyses revealed the composition of each crystal. Crystal **G**, which exhibits green monomer emission of perylene, was composed of the single diastereomer (*S*,*S*)-**1** and 1,4-dioxane, while **YG**, which shows yellow-green monomer emission, consisted of the diastereomers (*S*,*S*)-**1** and (*S*,*R*)-**1** along with toluene. In crystal **Y**, yellow excimer emission was observed due to the stacking of perylene moieties in (*S*,*S*)-**1** and (*S*,*R*)-**1**. Moreover, the application of mechanical and thermal stimuli to these crystals induced phase transitions to amorphous states that exhibit yellow-green emission. To the best of our knowledge, this is the first report on the production of three luminescent crystals from the dynamic diastereomers of a single compound. The strategy of utilizing dynamic diastereomers to achieve multi-color luminescent crystals serves as a novel approach and is expected to be applicable to other molecular systems, paving the way for the development of diverse luminescent organic crystals.

This work was partly supported by JST, PRESTO Grant Number JPMJPR21A3, Japan and JSPS KAKENHI Grant Numbers JP20K05645 within the Grant-in-Aid for Scientific Research (C), JP24K01451 within the Grant-in-Aid for Scientific Research (B), and JP24K21781 within the Grant-in-Aid for Challenging Research (Pioneering).

Conflicts of interest

There are no conflicts to declare.

Data availability

The data supporting this article have been included in the ESI.† Crystallographic data for **G**, **YG**, and **Y** have been deposited at the CCDC under deposition numbers 2422979–2422981 and can be obtained from https://www.ccdc.cam.ac.uk.

Notes and references

1 (a) P. Gayathri, M. Pannipara, A. G. Al-Sehemi and S. P. Anthony, *CrystEngComm*, 2021, **23**, 3771; (b) E. Li, K. Jie, M. Liu, X. Sheng, W. Zhu and F. Huang, *Chem. Soc. Rev.*, 2020, **49**, 1517; (c) M. Kato, H. Ito, M. Hasegawa and K. Ishii, *Chem. – Eur. J.*, 2019, **25**, 5105.

2 (a) Z. Zhao, Y. Cai, Q. Zhang, A. Li, T. Zhu, X. Chen and W. Z. Yuan, *Nat. Commun.*, 2024, **15**, 5054; (b) Y. Fujimoto, Y. Mochiduki, H. Sotome, R. Shimada, H. Okajima, Y. Toda, A. Sakamoto, H. Miyasaka and F. Ito, *J. Am. Chem. Soc.*, 2024, **146**, 32529; (c) R. Yoshida, T. Tachikawa and S. Ito, *Cryst. Growth Des.*, 2022, **22**, 547; (d) M. Shimizu, K. Nishimura, R. Hirakawa and T. Sakurai, *Chem. –Eur. J.*, 2021, **27**, 1626; (e) S. Ito, *Chem. Lett.*, 2021, **50**, 649; (f) S. Ito, S. Nagai, T. Ubukata, T. Ueno and H. Uekusa, *Cryst. Growth Des.*, 2020, **20**, 4443; (g) S. Feng, S. Gong and G. Feng, *Chem. Commun.*, 2020, **56**, 2511; (h) S. Takahashi, S. Nagai, M. Asami and S. Ito, *Mater. Adv.*, 2020, **1**, 708; (i) S. Ito, C. Nishimoto and S. Nagai, *CrystEngComm*, 2019, **21**, 5699; (j) J. Wu, Y. Cheng, J. Lan, D. Wu, S. Qian, L. Yan, Z. He, X. Li, K. Wang, B. Zou and J. You, *J. Am. Chem. Soc.*, 2016, **138**, 12803; (k) T. Seki, Y. Takamatsu and H. Ito, *J. Am. Chem. Soc.*, 2016, **138**, 6252; (l) X. Cheng, K. Wang, S. Huang, H. Zhang, H. Zhang and Y. Wang, *Angew. Chem., Int. Ed.*, 2015, **54**, 8369; (m) X. Y. Shen, Y. J. Wang, E. Zhao, W. Z. Yuan, Y. Liu, P. Lu, A. Qin, Y. Ma, J. Z. Sun and B. Z. Tang, *J. Phys. Chem. C*, 2013, **117**, 7334; (n) M. Shimizu, Y. Takeda, M. Higashi and T. Hiyama, *Angew. Chem., Int. Ed.*, 2009, **48**, 3653.

3 (a) Y.-H. Yang, Y.-S. Chen, W.-T. Chuang and J.-S. Yang, *J. Am. Chem. Soc.*, 2024, **146**, 8131; (b) Y. Yano, H. Kasai, Y. Zheng, E. Nishibori, Y. Hisaeda and T. Ono, *Angew. Chem., Int. Ed.*, 2022, **61**, e202203853; (c) M. Fukushima, K. Sato, Y. Fujimoto, F. Ito and R. Katoh, *Cryst. Growth. Des.*, 2022, **22**, 2071; (d) S. Ito, *CrystEngComm*, 2022, **24**, 1112; (e) S. Ito, S. Nagai, T. Ubukata, T. Tachikawa, *CrystEngComm*, 2021, **23**, 5899; (f) J.-Y. Zhu, C.-X. Li, P.-Z. Chen, Z. Ma, B. Zou, L.-Y. Niu, G. Cui and Q.-Z. Yang, *Mater. Chem. Front.*, 2020, **4**, 176; (g) G. Huang, Y. Jiang, S. Yang, B. S. Li and B. Z. Tang, *Adv. Funct. Mater.*, 2019, **29**, 1900516; (h) J. Guan, F. Xu, C. Tian, L. Pu, M.-S. Yuan and J. Wang, *Chem. –Asian J.*, 2019, **14**, 216; (i) M. Okazaki, Y. Takeda, P. Data, P. Pander, H. Higginbotham, A. P. Monkman and S. Minakata, *Chem. Sci.*, 2017, **8**, 2677; (j) A. Pick, M. Klues, A. Rinn, K. Harms, S. Chatterjee and G. Witte, *Cryst. Growth Des.*, 2015, **15**, 5495.

4 (a) K. Yuhara and K. Tanaka, *Angew. Chem., Int. Ed.*, 2024, **63**, e202319712; (b) C.-Y. Tsai, C.-M. Cheng, Y.-C. Ho, Y.-F. Hsu, Y.-H. Liu, S.-M. Peng and J.-S. Yang, *J. Chin. Chem. Soc.*, 2022, **69**, 1719; (c) S. Ma, Y. Liu, J. Zhang, B. Xu and W. Tian, *J. Phys. Chem. Lett.*, 2020, **11**, 10504.

5 (a) T. Yagi, T. Tachikawa and S. Ito, *CrystEngComm*, 2023, **25**, 2379; (b) S. Nagai, M. Yamashita, T. Tachikawa, T. Ubukata, M. Asami and S. Ito, *J. Mater. Chem. C*, 2019, **7**, 4988.

6 (a) P. Jiang, A. S. Mikherdov, H. Ito and M. Jin, *J. Am. Chem. Soc.*, 2024, **146**, 12463; (b) K. Wada, M. Suzuki, T. Kakuta, T. Yamagishi, S. Ohtani, S. Fa, K. Kato, S. Akine and T. Ogoshi, *Angew. Chem., Int. Ed.*, 2023, **62**, e202217971; (c) Q. Zhang, R. Toyoda, L. Pfeifer and B. L. Feringa, *J. Am. Chem. Soc.*, 2023, **145**, 6976; (d) H. Wang, W. Yang, K. K. Baldridge, C.-H. Zhan, T. U. Thikekar and A. C.-H. Sue, *Chem. Sci.*, 2021, **12**, 10985.

7 F. Yang, S. Wei, C.-A. Chen, P. Xi, L. Yang, J. Lan, H.-M. Gau and J. You, *Chem. Eur. J.*, 2008, **14**, 2223.

8 A. R. Karikachery, H. B. Lee, M. Masjedi, A. Ross, M. A. Moody, X. Cai, M. Chui, C. D. Hoff and P. R. Sharp, *Inorg. Chem.*, 2013, **52**, 4113.

9 Y. Shen, Z. Zhang, H. Liu, Y. Yan, S. Zhang, B. Yang and Y. Ma, *J. Phys. Chem. C*, 2019, **123**, 13047.

Data Availability Statement

The data supporting this article have been included in the ESI.† Crystallographic data for **G**, **YG**, and **Y** have been deposited at the CCDC under deposition numbers 2422979–2422981 and can be obtained from https://www.ccdc.cam.ac.uk.